https://doi.org/10.1016/j.engstruct.2020.111520

Design of Fixed-Ended Octagonal Shaped Steel Hollow Sections in Compression

Junbo Chen[1,2], Han Fang[3], Tak-Ming Chan[1,2]*

[1]Department of Civil and Environmental Engineering, The Hong Kong Polytechnic University, Hung Hom, Hong Kong, China
[2]Chinese National Engineering Research Centre for Steel Construction (Hong Kong Branch), The Hong Kong Polytechnic University, Hung Hom, Hong Kong, China
[3]School of Civil, Environmental and Mining Engineering, The University of Adelaide, South Australia 5005, Australia
*Corresponding author: tak-ming.chan@polyu.edu.hk

Abstract: In recent years, octagonal steel hollow sections (OctHSs) have attracted significant interest from researchers and engineers, and OctHSs have been employed in civil engineering applications. However, designs of OctHSs are not included in structural steel design codes. This paper therefore presents comprehensive numerical analyses on the stub column behaviour of OctHSs. A database of 46 stub column tests reported in 6 sources were collected. Different fabrication routes, steel grades and cross-sectional slenderness were covered. Finite element (FE) modelling was carried out to replicate the test observations. The validated FE models were subsequently adopted to conduct an extensive parametric study to supplement the test database. Existing design methods in North American specifications, ASCE standard, Eurocode, Australian code and recently published literature were thoroughly discussed and evaluated. It was found that existing design methods are not applicable to the design of OctHSs. New cross-sectional slenderness limits and modifications to the existing design methods were then proposed. The cross-sectional resistance obtained from different design methods were compared with test and FE results. The applicability of the modified design methods was confirmed by statistical analyses. The reliability of the modified design methods was finally verified through reliability analyses. Results indicate that the modified design methods can be used to accurately predict the resistance of OctHSs with accepted safety levels.

Keywords: Stub column; Welded section; Cold-formed section; Octagonal hollow section; Finite element model; Design.

1. Introduction

Steel hollow sections such as circular hollow sections (CHSs) and square/rectangular hollow sections (SHSs/RHSs) have been widely applied in constructions because of their aesthetic appearance and excellent structural behaviours [1]. In recent years, polygonal steel hollow sections, in particular octagonal hollow sections (OctHSs), have also attracted significant interest from researchers and engineers. They have been adopted in civil applications such as transmission poles, telegraph towers and lattice structures [2-4]. Fig. 1 depicts some lighting columns using OctHSs. When compared to SHS/RHS counterparts, the flat side width of an OctHS is smaller provided

they have the same perimeter. OctHSs therefore exhibit stronger local buckling resistances than those of SHSs/RHSs [3, 4]. In addition, flat surfaces in OctHSs provide easier beam-to-column connection construction as compared to CHSs [3].

To form an OctHS, there are three commonly used fabrication routes as discussed in Fang et al. [5]. The three routes could be classified into two categories: welded section (W) and cold-formed section. The welded section is formed by welding eight flat plates, while the cold-formed section is fabricated by welding two cold-formed half-sections at two corners (CF1) or at two flat surfaces (CF2), as shown in Fig. 2. To achieve an efficient structural design to promote the use of OctHS members, experimental and numerical studies have been conducted. Aoki et al. [6] and Mitiga et al. [7] experimentally investigated the local buckling strength of both welded and cold-formed OctHSs (CF2) through 6 stub column tests. Yield strengths of the steel plates employed in [6, 7] were 289 MPa and 307 MPa. Following the works in [6, 7], Migita and Fukumoto [8] analytically investigated the local buckling of polygonal sections and design equations for local buckling strength of OctHSs were proposed. Godat et al. [9] tested 2 cold-formed OctHS (CF1) stub column specimens, and a design equation was also proposed based on test results to estimate the cross-sectional resistance of OctHSs. In these studies [6-9], the material properties at corners were not examined and reported. Hence, the beneficial effect of strength enhancements at corners due to the cold-forming process was not accounted for. As suggested in Karren [10], the area of corner regions in SHSs/RHSs makes up 5% ~ 30% of the cross-sectional gross area. Similar percentage of corner areas could also be expected in OctHSs. Therefore, the influence of the strength enhancement should be taken into account in calculations of cross-sectional resistance to yield an economical cross-sectional design. Recently, experimental research on material properties at both flat and corner portions of OctHSs has been carried out on S355 steel [11], Q460 steel [4] and S690 steel [3]. A design formula to calculate the enhancement of yield strengths was proposed in [4] on the basis of these material tests. Corresponding stub columns tests were subsequently conducted. Both experimental and numerical studies on cold-formed OctHSs (CF2) using S355 steel with measured yield strength of 379 MPa were conducted by Zhu et al. [11]. Chen et al. [12] tested the stub column behaviour of 16 cold-formed OctHSs (CF1 and CF2) which were made of Q460 steel. Fang et al. [5] carried out a test programme consisting of 18 stub column specimens fabricated using S690 steel. Both welded sections and cold-formed sections were covered. To date, design rules for OctHSs have been specified in an ASCE standard for steel transmission pole structures ASCE/SEI 48-11 [13]. However, design of OctHSs is not included in any currently used structural steel design specifications like EN 1993-1-1 [14] and ANSI/AISC 360-16 [15]. And it was found in [5, 12] that the design method in ASCE/SEI 48-11 needs to be tightened as some slender sections are classified as non-slender sections using the specified slenderness limit.

This paper therefore aims at developing effective design methods in accordance with current steel design codes. Experimental test results reported in the literature were firstly collected. Finite

element (FE) models were then developed and validated against the collected test results. An extensive parametric study on stub column behaviour of OctHSs was subsequently conducted to supplement the limited test results of the stub columns in the literature. Both welded and cold-formed sections were covered. Current design methods for OctHSs or SHSs/RHSs in North American specifications, ASCE standard, Australian code, Eurocode and literature were discussed and evaluated. Modified design methods that are applicable to both normal strength steel and high strength steel with nominal yield strength ranging from 235 MPa to 690 MPa were proposed. Reliability analyses were finally carried out to check the reliability of the modified design methods.

2. Geometry of octagonal hollow sections

Geometries of octagonal hollow sections (OctHSs) formed through different fabrication routes are presented in Fig. 3. For a regular OctHS, the relation between flat side width B and overall width H is formulated by Eq. (1). The mid-surface flat width b_p of OctHSs is determined from Eq. (2), where h_p is overall width of the mid-surface and t is thickness of the tube.

$$B=H/\left(1+\sqrt{2}\right) \tag{1}$$

$$b_p=h_p/\left(1+\sqrt{2}\right)=\left(H-t\right)/\left(1+\sqrt{2}\right) \tag{2}$$

The internal side width b of welded and cold-formed OctHSs can be obtained by Eq. (3) and Eq. (4), respectively.

$$b = B\text{-}2t\cdot\tan\theta \tag{3}$$

$$b = B\text{-}2r_o\cdot\tan\theta = B\text{-}2(t+r_i)\cdot\tan\theta \tag{4}$$

in which θ is interior angle of OctHSs, equal to $\pi/8$, and r_o and r_i are corner radii of outer and inner surfaces. It is noted that the inner corner radius of welded sections is zero ($r_i = 0$). Eq. (3) actually is a special case of Eq. (4) and gives the same result. Cross-sectional areas of welded and cold-formed OctHSs are calculated from Eqs. (5) and (6).

$$A = 8\times b_p\times t \tag{5}$$

$$A = 8\times b\times t+\pi\left(r_o^2-r_i^2\right) \tag{6}$$

3. Summary of experimental database

Results of 46 experimental tests on OctHS stub columns reported in 6 sources [5, 6, 9, 11, 12, 16] were collected. All the stub column tests were conducted under a displacement-controlled manner

with fixed-ended conditions. Table 1 summarises the detailed information of each stub column test including designations and fabrication routes of specimens, overall width H, flat side width B, thickness of the tube t, length of the column L, outer and inner radii r_o and r_i, respectively, reported yield strengths or 0.2% proof strengths of flat and corner portions $f_{y,f}$ and $f_{y,c}$, and ultimate axial load N_u. A wide range of steel grades with $f_{y,f}$ ranging from 265 to 780 MPa was covered. The ranges of B and t in the test database are $59.6 \leq B \leq 300$ and $1.37 \leq t \leq 9.97$, achieving a B/t ratio varying from 7.4 to 66.7. Though 46 test results were collected, the number of the tests on OctHS stub columns still remains limited as many parameters affect the cross-sectional resistance. Therefore, to develop safe and effective design methods, extensive numerical analyses were conducted to replicate the tests and supplement the limited test results.

4. Numerical analyses

Numerical analyses by means of finite element (FE) modelling were carried out using commercially available finite element software package ABAQUS [17]. Test observations of the collected stub column specimens in Table 1 were firstly replicated to validate the FE models, and the validated FE models were subsequently adopted to conduct an extensive parametric study covering wide ranges of parameters.

4.1 Finite element models

Four-node shell elements with reduced integration, S4R, which have been extensively used to predict the structural responses of steel hollow sections in previous studies [5, 11, 12], were chosen in this study. Whole cross-section dimension of each stub column was modelled using the measured geometries. For cold-formed sections, an outer corner radius of $3t$ and an inner corner radius of $2t$ were used (based on statistical analyses of the collected results) if these values were not reported in the literature. With respect to the boundary condition, both ends of the stub columns were fully restrained against all degrees of freedom except for the axial translation at the loaded end. The axial load was applied by displacement increments utilising the "Static, general" function available in ABAQUS. Mesh convergence studies were conducted to determine a suitable mesh size for analyses. The mesh sensitivity studies show that a mesh size of $B/10$ for both longitudinal and transverse directions yields suitably accurate predictions while maximizing computational efficiency at the same time, where B is the side width of OctHSs. Measured material properties were incorporated in FE models. The input material behaviour is specified by multilinear stress-strain curves defined in terms of true stress and log plastic strain. The true stress and log plastic strain were converted from engineering stress-strain curves according to the recommendation of ABAQUS user's manual [17] as follows:

$$\sigma_T = \sigma_{Eng}\left(1+\varepsilon_{Eng}\right) \quad (7)$$

$$\varepsilon_p = \ln\left(1+\varepsilon_{Eng}\right) - \sigma_T / E \quad (8)$$

where σ_T and σ_{Eng} are true and engineering stresses respectively, ε_{Eng} is engineering strain, ε_p is logarithmic plastic strain and E is elastic modulus of steel. In the FE models, strength enhancement at corners is allowed for. It was found in Chen et al. [12] that FE models with corner properties extended to a width of thickness t beyond the curved portions produce best agreements with test results. Therefore, in this study the corner material properties were assigned to corner portions and to extended corner regions as shown in Fig. 4.

The lowest elastic buckling mode generated from linear elastic buckling analyses for all the stub columns investigated in this study was local buckling. It was taken as the profile of initial geometrical imperfection to simulate the distribution of local imperfection, examples of which is shown in Fig. 5. The measured maximum imperfection amplitude ω_0 of each specimen was used. As per ANSI/AISC 360-16 [15], for doubly symmetric closed sections, such as CHSs, SHSs and RHSs, under compression, the limit states are flexural buckling and local buckling. The OctHSs investigated in this study are also doubly symmetric sections. Although distortional buckling may occur in OctHS columns [18], it is not considered herein because preliminary numerical simulations showed that it is never critical for the cross-section geometries considered in this work. In addition, the OctHS columns are stub columns which were designed short enough to avoid flexural buckling. Therefore, the limit state of the OctHS stub columns in design is local buckling, which is in line with the numerical modelling results.

Membrane residual stresses were explicitly defined in the FE models with the magnitudes estimated from the predictive models proposed in Fang et al. [5] and Chen et al. [12]. Typical residual stress distributions in welded section (S690) and cold-formed section (Q460) incorporated in the FE models are depicted in Fig. 6. Positive values indicate tensile membrane residual stresses while negative values indicate compressive membrane residual stresses. To investigate the effect of residual stresses, FE models were conducted with and without residual stresses while other parameters remained the same. Fig. 7 presents the normalised axial load versus axial strain curves. Residual stresses affect the stub column behaviour of welded sections with 2% ~ 4% differences observed in the ultimate load. However, the axial load versus end shortening curves of cold-formed sections with and without residual stresses were almost identical, indicating the effect of residual stresses on cold-formed sections is negligible. Residual stresses were therefore taken into account in welded sections, but not incorporated in cold-formed sections.

4.2 Validation of FE models

Failure modes, ultimate axial loads and normalised axial load *versus* axial strain curves generated by FE models were compared with those obtained from experimental tests to assess the accuracy of the models. Fig. 8 shows the failure modes of OctHS stub columns observed from test results and FE models. The failure modes generated from FE models are shown to closely match the test observations. Comparisons of normalised axial load (N/Af_y) *versus* axial strain curves of the stub column tests are displayed in Fig. 9. It is worth noting that in the following sections without further notice f_y refers to yield strength of flat portions for welded sections and weighted average (by area) yield strength for cold-formed sections. The normalised axial load *versus* axial strain curves predicted from FE models were found to correlate well with that of test results. Ultimate loads obtained from FE models are summarised and compared to test results in Table 1. The mean value of Test N_u / FE N_u of all samples of OctHS stub columns is 1.01 with corresponding CoV of 0.02. It can be concluded that the test observations are accurately replicated in terms of failure modes, ultimate axial loads, and normalised axial load *versus* axial strain curves through the developed FE models.

4.3 Parametric study

With satisfactory ability to replicate test observations, the validated FE models were adopted to carry out a parametric study, aiming at generating FE results to supplement the test results covering broader ranges of cross-sectional slenderness and steel yield strengths. Both welded and cold-formed sections were covered in the parametric study. For welded sections, steel grades of S235, S355, S460, S550 and S690 hot-finished steels were used. The values of elastic modulus E, yield strength f_y, and ultimate strength f_u were taken in accordance with EN 1993-1-1 [14] and EN 1993-1-12 [19], and the ultimate strain at ultimate strength (ε_u) was determined by a predictive equation proposed by Yun and Gardner [20]. The bilinear plus nonlinear hardening material constitutive model for hot-finished steel proposed in [4] was adopted to obtain the stress-strain curves. As for cold-formed sections, material properties and stress-strain curves of S355, Q460 and S690 cold-formed steel reported by Zhu et al. [11], Chen et al. [12] and Fang et al. [5] respectively were employed. Tables 2 and 3 summarise the material parameters of hot-finished and cold-formed steels adopted in the parametric study. Fig. 10 depicts the stress-strain curves of all the steels used in the parametric study. A local geometrical imperfection amplitude of $0.1t$ [11], an outer corner radius of $3t$ and an inner corner radius of $2t$ for cold-formed sections [12] were adopted based on statistical analyses of the collected test specimens. It should be noted that membrane residual stresses were only considered in welded sections. For each steel grade, 30 FE models with different cross-sectional slenderness were built. Variations in the cross-sectional slenderness were achieved through gradually modifying the material thickness (from 1 mm to 9.26 mm), thereby giving different b_p/t ratios ranging from 8.0 to 74.8. Therefore, a total of 240 FE models were developed in the parametric study. Examples of FE results (32 out of 240) are reported in Table 4. The

parametric study results are used in parallel with test results to assess the current design methods for OctHSs under axial compression.

5. Design of octagonal steel hollow sections

5.1 Cross-sectional slenderness limits

In current design specifications, the concept of cross-section classification and the effective width (or effective strength) method are commonly adopted for the design of steel hollow sections. For cross-sections under axial compression, the cross-sections that can reach the yield strength are classified as Class 1-3 (or non-slender) sections, whilst those with local buckling occurred in the elastic stage before the yield strength are considered as Class 4 (or slender) sections. Maximum side width-to-thickness ratios b/t, also termed as cross-sectional slenderness, are stipulated in current design specifications for compression parts with flat elements.

ASCE/SEI 48-11 specifies a b/t limiting value for the design of OctHSs. However, designs of OctHSs are not included in current steel structure design codes such as ANSI/AISC 360-16 [15], AISI S100-16 [21], AS/NZS 4600 [22], AS 4100-1998(R2016) [23], EN 1993-1-1 [14] and EN 1993-1-5 [24]. Hence, slenderness limits for SHSs/RHSs specified in these specifications are discussed. It is noted that AS/NZS 4600 uses the same design approach as AISI S100-16. AS/NZS 4600 is therefore not repeatedly discussed in this study. It was found by Zhu et al. [11], Fang et al. [5] and Chen et al. [12] that current cross-sectional slenderness limit in different codes is not suitable for the design of OctHSs. New cross-sectional slenderness limits were therefore proposed for effective designs of OctHSs. Table 5 summarises the limits in which a normalised slenderness parameter $\bar{\lambda} = (b/t)\sqrt{f_y/E}$ is used to standardise the comparison between the codes and literature.

Based on the normalised plate slenderness $\bar{\lambda}$, ASCE/SEI 48-11 gives the largest slenderness limit of 1.52. ANSI/AISC 360-10, AS 4100-1998(R2016) and EN 1993-1-1 have similar slenderness limits of 1.40, 1.41, and 1.41, respectively. It is noted that design codes for cold-formed steel structure AISI S100 and EN 1993-1-5 have the same yield slenderness limit of 1.28. Smaller slenderness limits for the design of OctHSs have also been proposed in literature [5, 11, 12]. The suitability of the slenderness limits needs to be further verified to produce safe and economic predictions. The ultimate load N_u of the test and FE results is normalised by the yield load $N_y=Af_y$ and plotted with respect to the normalised slenderness parameter $\bar{\lambda} = (b/t)\sqrt{f_y/E}$, as shown Fig. 11. As indicated from Fig. 11, current slenderness limits in ASCE/SEI 48-11, AISI S100-16 (EN 1993-1-5), ANSI/AISC 360-16 (AS 4100-1998(R2016) and EN 1993-1-1) are unsafe. A new slenderness limit of $\bar{\lambda}$ = 1.11 was then proposed on the basis of regression analyses.

5.2 Evaluation of existing design methods and design recommendations

5.2.1 Effective width method

Effective width method (EWM) is commonly adopted in current design codes for the design of slender sections with plate elements. It has been standardised in AISI S100-16, ANSI/AISC 360-16, AS 4100-1998(R2016) and EN 1993-1-5. The original Winter's effective width formula is $\rho = b_e/b = 1.9(t/b)\sqrt{E/f_y}\,[1\text{-}0.415(t/b)\sqrt{E/f_y}\,] \le 1$, in which ρ is the reduction factor and b_e is effective width. The Winter's formula can be simplified as Eq. (9), in which λ_p is plate slenderness obtained from Eq. (10). The simplified Winter's effective width formula is adopted in AISI S100-16, ANSI/AISC 360-16 and EN 1993-1-5. The elastic buckling strength f_{cr} could be determined by plate buckling theory as presented in Eq. (11), where E is the elastic modulus, v is the Poisson's ratio of steel, b is the internal side width (excluding curved portion), t is the thickness of the tube and k is the plate buckling coefficient taken as 4.

$$\rho_{\text{AISI,AISC,EC3}} = \begin{cases} 1 & \text{for } \lambda_p \le 0.673 \\ \left(1 - 0.22/\lambda_p\right)/\lambda_p & \text{for } \lambda_p > 0.673 \end{cases} \tag{9}$$

$$\lambda_p = \sqrt{f_y / f_{cr}} \tag{10}$$

$$f_{cr} = k\frac{\pi^2 E}{12(1-v^2)}\left(\frac{t}{b}\right)^2 \tag{11}$$

In AS 4100-1998(R2016), Eq. (12) is used to determine the reduction factor ρ.

$$\rho_{\text{AS4100}} = 40/\left(\frac{b}{t}\sqrt{\frac{f_y}{250}}\right) \quad \text{for } b/t > 40\sqrt{250/f_y} \tag{12}$$

Recently, Fang et al. [5] carried out experimental and numerical analyses on high strength steel OctHSs and proposed Eq. (13) to calculate the reduction factor ρ for the design of slender high strength steel OctHSs.

$$\rho_{\text{Fang}} = \frac{0.905}{\lambda_p} - \frac{0.201}{\lambda_p^{\,2}} \quad \text{for } \lambda_p > 0.521 \tag{13}$$

The normalised ultimate load $N_u/(Af_y)$ of the test and FE results is plotted against the plate slenderness λ_p in Fig. 12(a). Current design curves are also drawn. In the last section, a new slenderness limit was proposed based on the normalised slenderness parameter. This limit can be rearranged as $b/t = 33\sqrt{f_y/235}$ in line with Eurocode terminology and can also be converted to λ_p

= 0.585, which is adopted in this section as the limit for EWM. Based on this limit, the original EWM in AISI S100-16, ANSI/AISC 360-16 and EN 1993-1-5 can be modified as follows for the design of OctHSs, in which ψ is the stress ratio and is taken as 1.0 for pure compression.

$$\rho_{\text{AISI,AISC}}{}^{*}=\begin{cases}1 & \text{for } \lambda_{\text{p}}\le 0.585\\ \left(1.05-0.272/\lambda_{\text{p}}\right)/\lambda_{\text{p}} & \text{for } \lambda_{\text{p}}>0.585\end{cases} \tag{14}$$

$$\rho_{\text{EC3}}{}^{*}=\begin{cases}1 & \text{for } \lambda_{\text{p}}\le 0.5+\sqrt{0.075-0.068\psi}\\ \left(1.05-0.068\left(3+\psi\right)/\lambda_{\text{p}}\right)/\lambda_{\text{p}} & \text{for } \lambda_{\text{p}}>0.5+\sqrt{0.075-0.068\psi}\end{cases} \tag{15}$$

Results of the ultimate-to-prediction ratio ($N_{\text{u}}/N_{\text{u,pred}}$) of test and FE results obtained from EWM, AS 4100-1998(R2016), Fang et al. [5] and modified EWM (labelled as EWM*) are summarised in Table 6. The $N_{\text{u}}/N_{\text{u,pred}}$ with regard to slenderness λ_{p} diagram is presented in Fig. 12(b). The mean $N_{\text{u}}/N_{\text{u,pred}}$ ratio of EWM, AS 4100-1998(R2016), Fang et al. [5] and modified EWM are 1.01, 1.07, 1.10 and 1.02 with corresponding coefficient of variances (CoVs) of 0.06, 0.08, 0.06 and 0.06. It is noted that the mean $N_{\text{u}}/N_{\text{u,pred}}$ ratio of modified EWM is slightly greater than that of original EWM. This is because the original EWM stipulates a greater slenderness limit (λ_{p} = 0.673) than that of the modified EWM (λ_{p} = 0.585). Within this range (0.585 < λ_{p} < 0.673), the original EWM overestimates the resistance as some slender sections are classified as non-slender sections, resulting in a $N_{\text{u}}/N_{\text{u,pred}}$ ratio lower than unity.

5.2.2 ASCE/SEI 48-11

ASCE/SEI 48-11 provides a design equation for regular OctHSs under uniform compression, as expressed in Eq. (16), where A is gross cross-sectional area, $f_{\text{a,ASCE}}$ is effective compressive strength, f_{y} is steel yield strength, b is internal side width excluding corner portion and t is material thickness.

$$\frac{N_{\text{u,ASCE}}}{A}=f_{\text{a,ASCE}}=\begin{cases}f_{\text{y}} & \text{for } b/t\le 260\times\dfrac{2.62}{\sqrt{f_{\text{y}}}}\\ 1.42\,f_{\text{y}}\left(1.0-0.00114\dfrac{\sqrt{f_{\text{y}}}}{2.62}\dfrac{b}{t}\right) & \text{for } 260\times\dfrac{2.62}{\sqrt{f_{\text{y}}}}<b/t\le 351\times\dfrac{2.62}{\sqrt{f_{\text{y}}}}\\ f_{\text{cr}} & \text{for } b/t>351\times\dfrac{2.62}{\sqrt{f_{\text{y}}}}\end{cases} \tag{16}$$

The normalised ultimate load $N_u/(Af_y)$ of the test and FE results is plotted with regard to the slenderness $((b/t)\sqrt{f_y}/2.62$ in line with ASCE/SEI 48-11 as shown in Fig. 13(a). Current design curve is drawn as the dash line. It was observed from Fig. 13(a) that current slenderness limit of 260 in ASCE/SEI 48-11 is unsafe for the design of OctHSs and the current design equation tends to overpredict the resistance of slender OctHSs within a slenderness range while overpredicting the resistance for others. Hence, a new slenderness limit of 190 (equivalent to $\lambda_p = 0.585$) was proposed herein to yield safe and accurate strength predictions. Similar to the modified EWM, a new set of design equations were derived as given in Eq. (17) based on the proposed slenderness limit, in which $\lambda^* = ((b/t)\sqrt{f_y}/2.62)/325$ converted from the plate buckling theory.

$$\frac{N_{u,pro}}{A} = f_{a,pro} = \begin{cases} f_y & \text{for } b/t \le 190 \times \dfrac{2.62}{\sqrt{f_y}} \\ \left(1.05 - \dfrac{0.276}{\lambda^*}\right)\dfrac{1}{\lambda^*} & \text{for } b/t > 190 \times \dfrac{2.62}{\sqrt{f_y}} \end{cases} \quad (17)$$

As indicated in Fig. 13(a), the proposed design curve improves the strength prediction for slender sections. Results of the ultimate-to-prediction ratio ($N_u/N_{u,pred}$) of test and FE results obtained from ASCE/SEI 48-11 and the proposed design equation are summarised in Table 7. The $N_u/N_{u,pred}$ with respect to cross-sectional slenderness $((b/t)\sqrt{f_y}/2.62$ diagram is depicted in Fig. 13(b). The mean $N_u/N_{u,pred}$ ratio of the proposed method is improved from 1.07 to 1.02 with corresponding CoV improved from 0.21 to 0.06. It is clear that the proposed design equation yields more accurate and less scattered strength predictions for OctHSs as shown in Fig. 13(b).

5.2.3 Direct strength method

The direct strength method (DSM) was originally developed by Schafer and Peköz [25, 26] for the design of cold-formed sections with flat elements and it is currently incorporated in AISI S100-16. The DSM utilises an overall cross-sectional slenderness (λ_p), as defined in Eq. (10), to determine the cross-sectional capacity, in which f_{cr} is elastic buckling strength of a cross-section considering the interaction between plate elements within the cross-section. The cross-sectional elastic buckling strength f_{cr} can be determined from either plate buckling theory or numerical analyses such as finite element modelling or finite strip method. In this paper, f_{cr} the was obtained from finite strip analyses using the programme CUFSM [27]. It was found that by replacing the internal side width b in Eq. (11) by mid-surface side width b_p (as shown in Fig. 3) the plate buckling theory (as expressed in Eq. (18)) produces close results of f_{cr} to that of CUFSM. The DSM nominal resistance of cross-sections subjected to local buckling could be then determined from Eq. (19).

$$f_{cr} = k\frac{\pi^2 E}{12(1-\nu^2)}\left(\frac{t}{b_p}\right)^2 \tag{18}$$

$$N_{u,DSM} = \begin{cases} f_y A & \text{for } \lambda_p \le 0.776 \\ \left[\left(1-\frac{0.15}{\lambda_p^{0.8}}\right)\frac{1}{\lambda_p^{0.8}}\right] f_y A & \text{for } \lambda_p > 0.776 \end{cases} \tag{19}$$

345

346 Fig. 14(a) depicts the normalised ultimate load $N_u/(Af_y)$ versus the overall cross-sectional
347 slenderness λ_p diagram of the test and FE results. Current DSM design curve is also plotted as a
348 dash line. As can be seen from Fig. 14(a), current DSM slenderness limit of 0.776 is unconservative
349 for the design of OctHSs. In previous section, a new slenderness limit $\lambda_p = 0.585$ was proposed for
350 the modified EWM. In that case, internal side width b excluding curved portion is used to
351 determine the plate slenderness. However, in DSM mid-surface side width b_p is used to obtain the
352 overall cross-sectional slenderness λ_p. Therefore, a new slenderness of 0.62 was proposed for
353 modified DSM. Based on this limit, the original DSM in AISI S100-16 can be modified as Eq.
354 (20).
355

$$N_{u,DSM}{}^* = \begin{cases} f_y A & \text{for } \lambda_p \le 0.62 \\ \left[\left(1-\frac{0.227}{\lambda_p^{0.9}}/\right)\frac{1}{\lambda_p^{0.9}}\right] f_y A & \text{for } \lambda_p > 0.62 \end{cases} \tag{20}$$

356

357 In Fig. 14(a), it is obvious that the modified DSM (labelled as DSM*) improves the resistance
358 prediction for slender sections. Results of the ultimate-to-prediction ratio ($N_u/N_{u,pred}$) of test and
359 FE results obtained from original DSM and modified DSM are summarised in Table 8. The
360 $N_u/N_{u,pred}$ with respect to overall cross-sectional slenderness λ_p diagram is presented in Fig. 14(b).
361 The modified DSM yields more accurate and less scattered strength predictions for OctHSs. The
362 mean $N_u/N_{u,pred}$ ratio is improved from 0.97 to 1.02 with corresponding CoV improved from 0.08
363 to 0.06.
364

365 *5.2.4 Continuous strength method*

366

367 Similar to DSM, the continuous strength method (CSM), which was developed by Gardner and
368 Nethercot [28], also adopts the overall cross-section slenderness (λ_p) to classify the cross-sections.
369 To date, CSM has been developed for the design of cross-sections using normal strength carbon
370 steel [28-31] and high strength steel [32, 33]. To consider the beneficial effect of strain-hardening,
371 CSM relates the local buckling strain (also termed as CSM limiting strain) to the overall cross-
372 sectional slenderness, as shown in Eq. (21), where ε_{csm} is CSM limiting strain, ε_y is yield strain
373 equal to f_y/E, f_y is steel yield strength and E is steel elastic modulus.

$$\frac{\varepsilon_{csm}}{\varepsilon_y}=\begin{cases}\dfrac{0.25}{\lambda_p^{3.6}}\le \min(15,\dfrac{0.6\varepsilon_u}{\varepsilon_y}) & \text{for } \lambda_p \le 0.68\\ (1-\dfrac{0.222}{\lambda_p^{1.05}})\dfrac{1}{\lambda_p^{1.05}} & \text{for } \lambda_p > 0.68\end{cases} \tag{21}$$

The CSM limiting strength (f_{csm}) in compression is determined as follows:

$$f_{csm}=\begin{cases}E\varepsilon_{csm} & \text{for } \varepsilon_{csm}/\varepsilon_y \le 1.0\\ f_y+(\varepsilon_{csm}-\varepsilon_y)E_{sh} & \text{for } \varepsilon_{csm}/\varepsilon_y > 1.0\end{cases} \tag{22}$$

in which E_{sh} is modulus of strain-hardening. E_{sh} is defined in Eq. (23), where f_u is the ultimate strength and ε_u is the ultimate strain at ultimate strength. To avoid excessive plastic strain and consider the effect strain-hardening in appropriate extent in design, two upper limits ($15\varepsilon_y$ and $0.4\varepsilon_u$) [30, 31] are stipulated to the CSM limiting strain (ε_{csm}) for non-slender cross-sections.

$$E_{sh}=\frac{f_u-f_y}{0.45\varepsilon_u-\varepsilon_y} \tag{23}$$

The CSM capacity of non-slender and slender cross-sections in compression (N_{csm}) can be determined using Eq. (24). Due to the existence of pronounced yield plateau in the welded sections, CSM is only applied to cold-formed steel sections to allow for strain-hardening.

$$N_{u,CSM}=f_{csm}A \tag{24}$$

Fig. 15(a) shows the normalised ultimate load $N_u/(Af_y)$ versus the overall cross-sectional slenderness λ_p diagram of slender section results. Current CSM design curve for slender sections is also presented as a dash line. As can be observed from Fig. 15(a), current CSM is conservative for the design of slender OctHSs when λ_p > 1.5. It is noted that the modified DSM for slender sections can be directly adopted herein and gives satisfactory predictions. The modified CSM is therefore given in Eq. (25).

$$N_{u,CSM}{}^{*}=\begin{cases}\left[f_y+(\varepsilon_{csm}-\varepsilon_y)E_{sh}\right]A & \text{for } \lambda_p \le 0.62\\ \left[\left(1-\dfrac{0.227}{\lambda_p^{0.9}}/\right)\dfrac{1}{\lambda_p^{0.9}}\right]f_yA & \text{for } \lambda_p > 0.62\end{cases} \tag{25}$$

Results of the ultimate-to-prediction ratio ($N_u/N_{u,pred}$) of cold-formed section results obtained from the original CSM and modified CSM are summarised in Table 9. The $N_u/N_{u,pred}$ with respect to overall cross-sectional slenderness λ_p diagram is presented in Fig. 15(b). It is obvious that the modified CSM produces more accurate and less scattered resistance predictions for OctHSs. The mean $N_u/N_{u,pred}$ ratio is improved from 1.03 to 1.02 with corresponding CoV improved from 0.04 to 0.03.

5.2.5 Summary

In general, the existing EWM, DSM and CSM are not applicable for OctHS stub columns, and the slenderness limits are unsafe to be adopted. In addition, the design method for OctHSs specified in ASCE/SEI 48-11 is unconservative as well. On the basis of the collected test database and FE results, modifications to these methods are recommended. The modified design methods have been proven to accurately and consistently predict the resistance of OctHS stub columns. Since the beneficial effect of strain-hardening is considered in CSM, it gives the best predictions among all the design methods.

5.3 Reliability analyses

The reliability of the modified EWM, proposed Eq. (17), DSM and CSM was assessed in accordance with North American specification ANSI/AISC 360-16. The reliability analysis was carried out based on a load combination of 1.2 × DL + 1.6 × LL and a LL/DL ratio of 3. DL and LL represent the dead load and live load, respectively. The equation for calculating reliability index β is expressed in Eq. (26),

$$\beta = \frac{\ln(R_m / Q_m)}{\sqrt{V_R^2 + V_Q^2}} = \frac{\ln((P_m M_m F_m) R_n / Q_m)}{\sqrt{(V_P^2 + V_M^2 + V_F^2) + V_Q^2}} \tag{26}$$

in which R_m and Q_m are mean resistance and mean load effect, V_R and V_Q are CoV of resistance and CoV of load effect, R_n is nominal resistance, P_m and V_P are mean ratio of experiment-to-predicted results and corresponding CoV, and M_m, F_m, V_M and V_F are mean-nominal yield strength, mean ratio of the actual section modulus to specified value, and corresponding CoVs, taken as the specified values in AISI S100-16. Key parameters for the reliability analyses are summarized in Table 10. When the safety factor ϕ is fixed as 0.9 in accordance with ANSI/AISC 360-16, reliability index β of all modified methods is greater than the target value of 2.6. When the value of reliability index β is fixed at 2.6, safety factors of 0.96, 0.96, 0.96 and 0.975 are obtained for the modified EWM, proposed Eq. (17), modified DSM and modified CSM, respectively. Therefore,

the modified design methods can accurately and consistently predict the resistance of OctHSs with an accepted safety level.

6. Conclusions

This paper has performed comprehensive numerical analyses on the stub column behaviour of welded and cold-formed OctHSs. A test database of 46 stub columns reported in 6 sources were firstly collected. Finite element (FE) models were then developed to replicate the test observations. By using the developed FE models, the test observations were accurately replicated in terms of failure modes, ultimate axial loads and normalised axial load *versus* axial strain curves. The validated FE models were subsequently adopted to conduct an extensive parametric study to supplement the test database. Steel grades from S235 to S690 and different fabrication routes, namely, welded sections and cold-formed sections, were considered.

The cross-sectional slenderness limits specified in current design methods, ANSI/AISC 360-16, AISI S100-16, ASCE/SEI 48-11, AS 4100-1998(2016), EN 1993-1 (EN 1993-1-1 and EN 1993-1-5), Fang et al. [5], DSM and CSM were evaluated against the test results together with the FE results. It was found that current limits in design standards are unsafe for the design of OctHSs. New cross-sectional slenderness limits in accordance with corresponding design methods were then proposed based on evaluation results. The cross-sectional resistance obtained from different design methods was compared with test and FE results. Generally, the existing effective width method, DSM and CSM are not applicable for OctHS stub columns, and the design method for OctHSs specified in ASCE/SEI 48-11 is unconservative. Modifications to the design methods were proposed to yield accurate and consistent predictions. The reliability of the modified design methods was finally verified through reliability analyses. Results indicate that the modified design methods can be used to accurately predict the resistance of OctHSs with accepted safety levels.

Acknowledgement

The research work presented in this paper was supported by a grant from the Research Grants Council of the Hong Kong Special Administrative Region, China (Project no. PolyU 152492/16E). The authors appreciate the support from the Chinese National Engineering Research Centre for Steel Construction (Hong Kong Branch) at The Hong Kong Polytechnic University.

Reference

[1] Wardenier J. “Hollow sections in structural applications”, 2nd ed. Geneva: CIDECT; 2011.

[2] Slocum R.M., Considerations in the design and fabrication of tubular steel transmission structures. Proceedings of the fifteenth international symposium on tubular structures – ISTS 15, 27–29 May 2015, Rio de Janeiro, Brazil. 2015.

[3] Fang H., Chan T.M., Young B., Material properties and residual stresses of octagonal high strength steel hollow sections, J Construct Steel Res, 2018; 184: 479-490.
[4] Chen J., Liu H., Chan T.M., Material properties and residual stresses of cold-formed octagonal hollow sections, J Construct Steel Res 2020; 170: 106078.
[5] Fang H., Chan T.M., Young B., Behavior of octagonal high strength steel tubular stub columns, J. Struct. Eng. (ASCE), 2019; 145(12): 04019150.
[6] Aoki T, Migita Y, Fukumoto Y. Local buckling strength of closed polygon folded section columns. J Constr Steel Res 1991; 20(4): 259–70.
[7] Migita Y., Aoki T., Fukumoto Y., Local and interaction buckling of polygonal section steel columns, J. Struct. Eng. 1992; 118: 2659–2676.
[8] Migita Y, Fukumoto Y. Local buckling behaviour of polygonal sections. J Constr Steel Res 1997 Feb 1; 41(2–3): 221–33.
[9] Godat A, Legeron F, Bazonga D. Stability investigation of local buckling behavior of tubular polygon columns under concentric compression. Thin-Walled Struct 2012; 1(53): 131–40.
[10] Karren K.W., Corner properties of cold-formed steel shapes, J Struct Div, ASCE 1967 93(ST1) 401-432.
[11] Zhu J.Y., Chan T.M., Young B., Cross-sectional capacity of octagonal tubular steel stub columns under uniaxial compression, Eng Struct, 2019; 184: 480-494.
[12] Chen J., Zhu J.Y., Chan T.M. Experimental and numerical investigation on stub column behaviour of cold-formed octagonal hollow sections. Eng Struct, 2020; 214: 110669.
[13] ASCE/SEI 48-11. Design of steel transmission pole structures, Reston, Virginia, American Society of Civil Engineers, 2011.
[14] EN 1993-1-1. Eurocode 3: Design of steel structures – Part 1.1: General rules and rules for buildings, European Committee for Standardization (CEN), Brussels; 2005.
[15] ANSI/AISC 360-16. “Specification for structural steel buildings”. Chicago, American Institute of Steel Construction (AISC); 2016.
[16] Zhu J.Y., Chan T.M., Behaviour of polygonal-shaped steel-tube columns filled with high-strength concrete. Proc Inst Civil Eng – Struct Build 2018; 171(2): 96–112.
[17] ABAQUS/Standard. Version 6.13-1. USA: K. a. S. Hibbit; 2013.
[18] Gonçalves R and Camotim D. Elastic buckling of uniformly compressed thin-walled regular polygonal tubes, Thin-Walled Struct., 2013, 71: 35-45.
[19] EN 1993-1-12. Eurocode 3: Design of steel structures-Part 1-12: additional rules for the extension of EN 1993 up to steel grades S700, European Committee for Standardization (CEN), Brussels; 2007.
[20] Yun X, Gardner L. Stress-strain curves for hot-rolled steels. J Construct Steel Res 2017; 133: 36–46.
[21] AISI S100-16. North American specification for the design of cold-formed steel structural members, Washington: American Iron and Steel Institute (AISI); 2016.
[22] AS/NZS 4600. Cold-formed steel structures. Sydney, Australia; 2018.

[23] AS 4100-1998(R2016). Steel structures (Reconfirmed 2016 Incorporating Amendment No.1). Sydney, Australia; 2016.
[24] EN 1993-1-5. Eurocode 3: Design of steel structures – Part 1.5: Plated structural elements. Brussels: European Committee for Standardization (CEN); 2006.
[25] Schafer BW, Peköz T. Direct strength predictions of cold-formed steel members using numerical elastic buckling solutions. In: Proceedings of the fourteenth international speciality conference on cold-formed steel structures. St. Louis (MO, USA); 1998.
[26] Schafer BW. Review: the direct strength method of cold-formed steel member design. J Construct Steel Res 2008; 64(7): 766–78.
[27] Schafer BW, Ádány S. Buckling analysis of cold-formed steel members using CUFSM: conventional and constrained finite strip methods. In: Proceedings of the eighteenth international speciality conference on cold-formed steel structures. Orlando (USA); 2006.
[28] Gardner L, Nethercot D. Structural stainless steel design: a new approach. Struct Eng 2004; 82: 2–28.
[29] Gardner L. The continuous strength method. Proc ICE – Struct Build 2008;161(3):127–33.
[30] Liew A, Gardner L. Ultimate capacity of structural steel cross-sections under compression, bending and combined loading. Struct 2015; 1: 2–11.
[31] Buchanan C, Gardner L, Liew A. The continuous strength method for the design of circular hollow sections. J Constr Steel Res 2016; 118: 207–16.
[32] Lan XY, Chen J, Chan TM, Young B. The continuous strength method for the design of high strength steel tubular sections in compression. Eng Struct 2018; 162: 177–87.
[33] Lan XY, Chen J, Chan TM, Young B. The continuous strength method for the design of high strength steel tubular sections in bending. J Constr Steel Res 2019; 160: 499–509.

Table 1. Experimental tests on OctHS stub columns.

Reference	Designation	Fabrication routes	H (mm)	B (mm)	t (mm)	L (mm)	r_o (mm)	r_i (mm)	$f_{y,f}$ (MPa)	$f_{y,c}$ (MPa)	Test N_u (kN)	FE N_u (kN)	Test N_u / FE N_u
Chen et al. [12]	O60×3-CF1	CF1	147.5	61.1	3.03	431	10.0	7.0	541	655	822	823	1.00
	O60×3-CF1#	CF1	147.1	60.9	3.05	432	9.5	7.0	541	655	831	830	1.00
	O60×3-CF2	CF2	146.8	60.8	3.04	434	10.0	7.0	541	655	830	826	1.01
	O60×3-CF2#	CF2	147.4	61.0	3.05	433	10.0	7.5	541	655	839	826	1.02
	O75×3-CF1	CF1	184.8	76.6	3.05	543	10.5	7.5	541	655	1031	1020	1.01
	O75×3-CF1#	CF1	184.8	76.6	3.04	542	10.0	7.0	541	655	1019	1008	1.01
	O75×3-CF2	CF2	184.4	76.4	3.05	544	10.0	7.0	541	655	1030	1024	1.01
	O75×6-CF1	CF1	183.5	76.0	5.83	543	19.0	13.5	581	735	2132	2227	0.96
	O75×6-CF1#	CF1	184.7	76.5	5.83	544	18.5	12.5	581	735	2141	2263	0.95
	O75×6-CF2	CF2	184.1	76.3	5.83	542	19.0	13.5	581	735	2153	2209	0.97
	O90×3-CF1	CF1	222.0	92.0	3.05	641	10.0	7.5	541	655	1180	1176	1.00
	O90×3-CF2	CF2	220.3	91.3	3.05	645	10.0	7.0	541	655	1181	1149	1.03
	O90×3-CF2#	CF2	220.4	91.3	3.06	647	10.5	7.5	541	655	1230	1169	1.05
	O105×3-CF1	CF1	257.8	106.8	3.05	756	10.0	7.0	541	655	1160	1163	1.00
	O105×3-CF1#	CF1	256.5	106.2	3.05	755	10.0	7.0	541	655	1191	1196	1.00
	O105×3-CF2	CF2	255.9	106.0	3.04	757	10.0	7.5	541	655	1207	1198	1.01
Fang et al. [5]	W-75×10a	W	179.1	74.2	9.93	498	0.0	0.0	780	780	4486	4513	0.99
	W-75×10b	W	180.6	74.8	9.86	501	0.0	0.0	780	780	4563	4520	1.01
	W-75×6a	W	179.4	74.3	6.24	499	0.0	0.0	764	764	2756	2748	1.00
	W-75×6b	W	178.4	73.9	6.00	499	0.0	0.0	764	764	2715	2730	0.99
	W-160×6a	W	385.3	159.6	6.05	1042	0.0	0.0	764	764	5239	5218	1.00
	W-160×6b	W	384.3	159.2	5.98	1041	0.0	0.0	764	764	5010	5009	1.00
	CF1-75×10a	CF1	179.1	74.2	9.92	501	25.0	15.3	753	780	4466	4428	1.01
	CF1-75×10b	CF1	178.2	73.8	9.95	497	25.0	15.1	753	780	4565	4584	1.00
	CF1-75×6a	CF1	178.9	74.1	6.20	499	20.6	14.0	762	775	2796	2842	0.98
	CF1-75×6b	CF1	177.4	73.5	6.17	498	19.4	13.5	762	775	2749	2785	0.99
	CF1-160×6a	CF1	383.1	158.7	6.02	1043	20.9	14.9	766	775	5504	5555	0.99
	CF1-160×6b	CF1	381.2	157.9	6.01	1043	21.0	15.0	766	775	5660	5675	1.00
	CF2-75×10a	CF2	178.9	74.1	9.97	501	25.0	15.0	759	773	4525	4495	1.01

	CF2-75×10b	CF2	178.7	74.0	9.91	498	25.0	15.0	759	773	4481	4442	1.01
	CF2-75×6a	CF2	177.4	73.5	5.88	494	20.2	14.8	760	796	2611	2600	1.00
	CF2-75×6b	CF2	181.1	75.0	5.90	496	20.1	14.2	760	796	2700	2651	1.02
	CF2-160×6a	CF2	385.5	159.7	6.02	1042	20.3	14.3	754	778	5489	5502	1.00
	CF2-160×6b	CF2	379.0	157.0	5.99	1044	20.4	13.7	754	778	5398	5414	1.00
Zhu et al. [11]	OctHS-1	CF2	178.0	73.7	5.55	695	16.7	11.1	379	548	1466	1496	0.98
	OctHS-2	CF2	178.0	73.7	5.54	695	16.6	11.1	379	548	1441	1441	1.00
	OctHS-3	CF2	178.0	73.7	5.53	695	16.6	11.1	379	548	1451	1466	0.99
Zhu and Chan [16]	O-H-1	CF2	143.9	59.6	3.10	449	9.3	6.2	296	-	449	442	1.02
Godat. et al. [9]	OCT-1-A	CF1	247.0	102.3	1.90	780	7.6	5.7	279	-	327	317	1.03
	OCT-4-A	CF1	194.0	80.4	1.37	780	5.5	4.1	265	-	198	195	1.02
Aoki et al. [6]	Oct-15	CF2	362.1	150.0	4.50	1200	13.5	9.0	289	-	278	273	1.02
	OCT15-b	CF2	362.1	150.0	4.50	1200	13.5	9.0	289	-	274	266	1.03
	OCT-15w	W	362.1	150.0	4.50	1200	0.0	0.0	289	-	275	267	1.03
	Oct-20	CF2	482.8	200.0	4.50	1200	13.5	9.0	289	-	244	239	1.02
	Oct-25	CF2	603.6	250.0	4.50	1200	13.5	9.0	289	-	206	194	1.06
	Oct-30	CF2	724.3	300.0	4.50	1200	13.5	9.0	289	-	173	160	1.08
Mean													1.01
CoV													0.02

Note: # indicates a repeated test.

Table 2. Material properties of hot-rolled steels.

Steel grade	E (GPa)	f_y (MPa)	f_u (MPa)	ε_u (%)
S235	210	235	360	20.8
S355	210	355	490	16.5
S460	210	460	550	9.82
S550	210	550	640	8.44
S690	210	690	770	6.23

Table 3. Material parameters of cold-formed steels.

Steel grade	Reference	Flat portion				Corner portion			
		$E_{s,f}$ (GPa)	$f_{y,f}$ (MPa)	$f_{u,f}$ (MPa)	$\varepsilon_{u,f}$ (%)	$E_{s,c}$ (GPa)	$f_{y,c}$ (MPa)	$f_{u,c}$ (MPa)	$\varepsilon_{u,c}$ (%)
S355	[11]	213	379	503	10.1	214	548	596	1.3
Q460	[12]	210	541	623	10.8	201	655	690	1.2
S690	[5]	210	762	802	4.1	191	775	825	1.2

Table 4. Representative OctHS stub column FE results.

Fabrication routes	Steel grades	h_p (mm)	b_p (mm)	t (mm)	r_o (mm)	r_i (mm)	b_p/t	b/t	N_u (kN)	f_{cr} (MPa)
Welded	235	178.8	74.06	4.63			16.0	15.2	654	2967
		178.8	74.06	2.85			26.0	25.2	396	1124
		178.8	74.06	2.06			36.0	35.1	281	587
		178.8	74.06	1.61			46.0	45.2	206	359
	355	178.8	74.06	4.63			16.0	15.2	989	2967
		178.8	74.06	2.85			26.0	25.2	593	1124
		178.8	74.06	2.06			36.0	35.1	405	587
		178.8	74.06	1.61			46.0	45.2	276	359
	460	178.8	74.06	4.63			16.0	15.2	1282	2967
		178.8	74.06	2.85			26.0	25.2	761	1124
		178.8	74.06	2.06			36.0	35.1	493	587
		178.8	74.06	1.61			46.0	45.2	320	359
	550	178.8	74.06	4.63			16.0	15.2	1530	2967
		178.8	74.06	2.85			26.0	25.2	895	1124
		178.8	74.06	2.06			36.0	35.1	555	587
		178.8	74.06	1.61			46.0	45.2	351	359
	690	178.8	74.06	4.63			16.0	15.2	1918	2967
		178.8	74.06	2.85			26.0	25.2	1100	1124
		178.8	74.06	2.06			36.0	35.1	645	587
		178.8	74.06	1.61			46.0	45.2	403	359
Cold-formed	355	178.8	74.06	4.63	13.9	9.3	16.0	13.9	1199	3010
		178.8	74.06	2.85	8.6	5.7	26.0	23.9	665	1140
		178.8	74.06	2.06	6.2	4.1	36.0	33.9	439	596
		178.8	74.06	1.61	4.8	3.2	46.0	43.9	286	364
	460	178.8	74.06	4.63	13.9	9.3	16.0	13.9	1563	2947
		178.8	74.06	2.85	8.6	5.7	26.0	23.9	895	1117
		178.8	74.06	2.06	6.2	4.1	36.0	33.9	544	583
		178.8	74.06	1.61	4.8	3.2	46.0	43.9	344	356
	690	178.8	74.06	4.63	13.9	9.3	16.0	13.9	2099	2967
		178.8	74.06	2.85	8.6	5.7	26.0	23.9	1175	1124
		178.8	74.06	2.06	6.2	4.1	36.0	33.9	665	587
		178.8	74.06	1.61	4.8	3.2	46.0	43.9	420	359

Table 5. Cross-sectional slenderness limits for OctHSs or SHSs/RHSs.

References	Slenderness limits	$\bar{\lambda}$
ASCE/SEI 48-11 [13]	$b/t \le 2.62\times 260/\sqrt{f_y}$, E = 200 GPa	1.52
AISI S100-16 [20]/ AS/NZS 4600 [21]	$\lambda_p \le \sqrt{f_y/f_{cr}} \le 0.673$, $f_{cr} = 4\dfrac{\pi^2 E}{12(1-\nu^2)}\left(\dfrac{t}{b}\right)^2$, E = 200 GPa, ν = 0.3	1.28
ANSI/AISC 360-16 [15]	$b/t \le 1.40\sqrt{E/f_y}$, E = 200 GPa	1.40
AS 4100 [22]	$b/t \le 40\sqrt{250/f_y}$, E = 200 GPa	1.41
EN 1993-1-1 [14]	$b/t \le 42\sqrt{235/f_y}$, E = 210 GPa	1.41
EN 1993-1-5 [23]	$\bar{\lambda}_p = \dfrac{b/t}{28.4\sqrt{k(235/f_y)}} \le 0.5+\sqrt{0.085-0.055\psi}$,ψ = 1 for pure compression, E = 210 GPa	1.28
Zhu et al. [11]	$b/t \le 29.8\sqrt{235/f_y}$ (S355 steel)	1.00
Fang et al. [5]	$b/t \le 30\sqrt{235/f_y}$ (S690 steel)	1.00
Chen et al. [12]	$b/t \le 34.1\sqrt{235/f_y}$ (Q460 steel)	1.14
DSM [24, 25]	$\lambda_p \le \sqrt{f_y/f_{cr}} \le 0.776$, $f_{cr} = 4\dfrac{\pi^2 E}{12(1-\nu^2)}\left(\dfrac{t}{b_p}\right)^2$, E = 200 GPa, ν = 0.3	1.34
CSM [26]	$\lambda_p \le \sqrt{f_y/f_{cr}} \le 0.68$, $f_{cr} = 4\dfrac{\pi^2 E}{12(1-\nu^2)}\left(\dfrac{t}{b_p}\right)^2$, ν = 0.3	1.29

Table 6. Comparison of test and FE results with EWM predictions.

Parameters	EWM	AS 4600	Fang et al. [5]	EWM*
Mean	1.01	1.07	1.10	1.02
CoV	0.06	0.08	0.06	0.06

Note: * indicates the modified method.

Table 7. Comparison of test and FE results with ASCE/SEI 48-11 predictions.

Parameters	ASCE/SEI 48-11			Proposed Eq. (17)		
	Non-slender	Slender	All	Non-slender	Slender	All
Mean	1.05	1.10	1.07	1.05	1.02	1.02
CoV	0.08	0.27	0.21	0.07	0.04	0.06

Table 8. Comparison of test and FE results with DSM predictions.

Parameters	DSM			DSM*		
	Non-slender	Slender	All	Non-slender	Slender	All
Mean	1.05	0.93	0.97	1.05	1.01	1.02
CoV	0.08	0.05	0.08	0.08	0.03	0.06

Note: * indicates the modified method.

Table 9. Comparison of test and FE results with CSM predictions.

Parameters	CSM			CSM*		
	Non-slender	Slender	All	Non-slender	Slender	All
Mean	1.02	1.04	1.03	1.02	1.03	1.02
CoV	0.03	0.04	0.04	0.03	0.03	0.03

Note: * indicates the modified method.

Table 10. Statistical parameters for the reliability analyses according to ANSI/AISC 360-16.

Results	EWM*	Eq. (17)	DSM*	CSM*
V_R	0.093	0.093	0.093	0.077
V_Q	0.19	0.19	0.19	0.19
ϕ	0.9	0.9	0.9	0.9
β	2.90	2.90	2.90	2.99
$\phi^{\#}$	0.96	0.96	0.96	0.975
$\beta^{\#}$	2.60	2.60	2.60	2.60

Note: No. of tests = 46; No. of FE = 240.

* indicates the modified method.

$^{\#}$ Reliability analyses yielding a reliability index of 2.60.

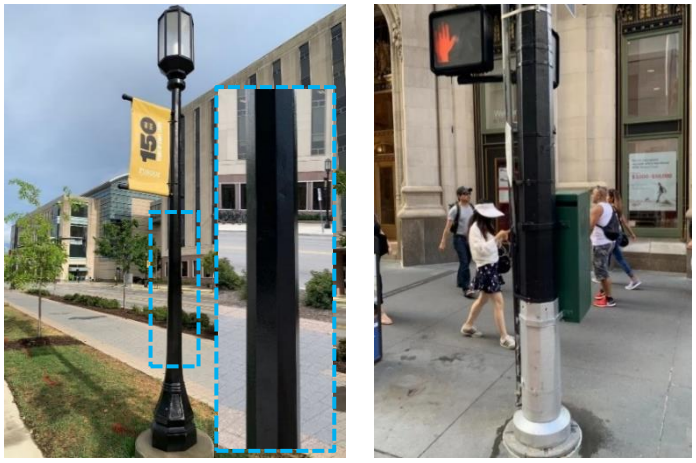

(a) West Lafayette, US [4] (b) New York, US [12]

Fig. 1. Octagonal section lighting columns.

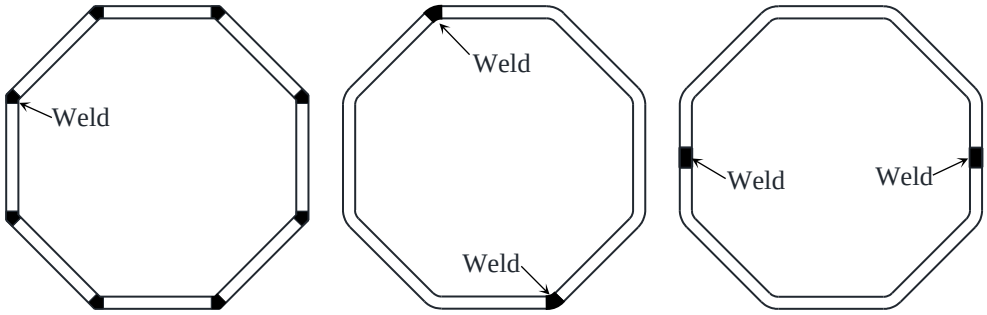

(a) Welded section (W) (b) CF1 (c) CF2

Fig. 2. Different fabrication routes for OctHSs.

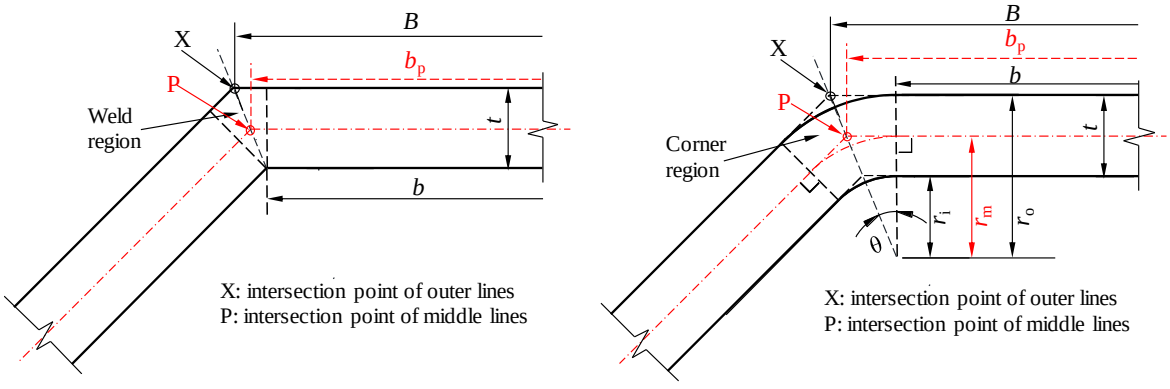

(a) Welded section (b) Cold-formed section

Fig. 3. Geometry of OctHSs and definition of symbols.

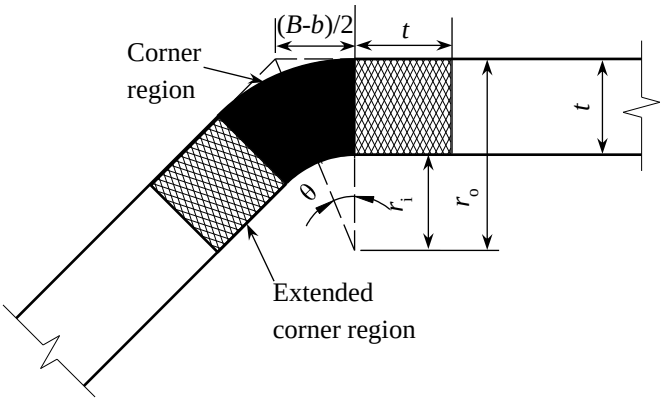

Fig. 4. Extents of corner regions of cold-formed OctHSs in FE.

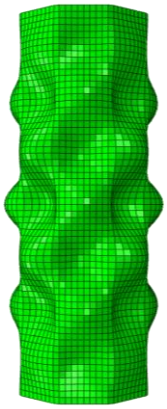

Fig. 5. The lowest eigenmode of OctHS stub columns.

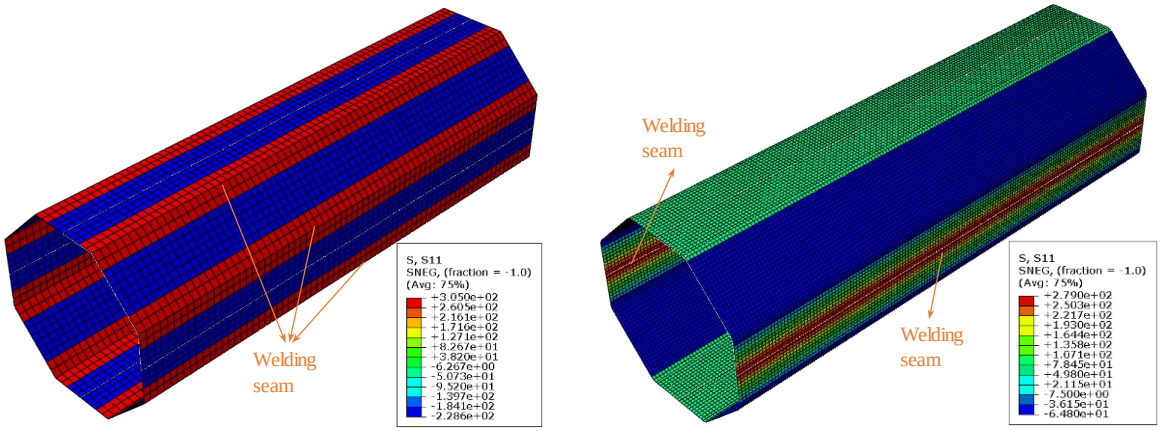

(a) Welded section (S690) (b) Cold-formed section (Q460)

Fig. 6. Typical residual stress distributions in FE models (positive and negative values indicate tensile and compressive stress.).

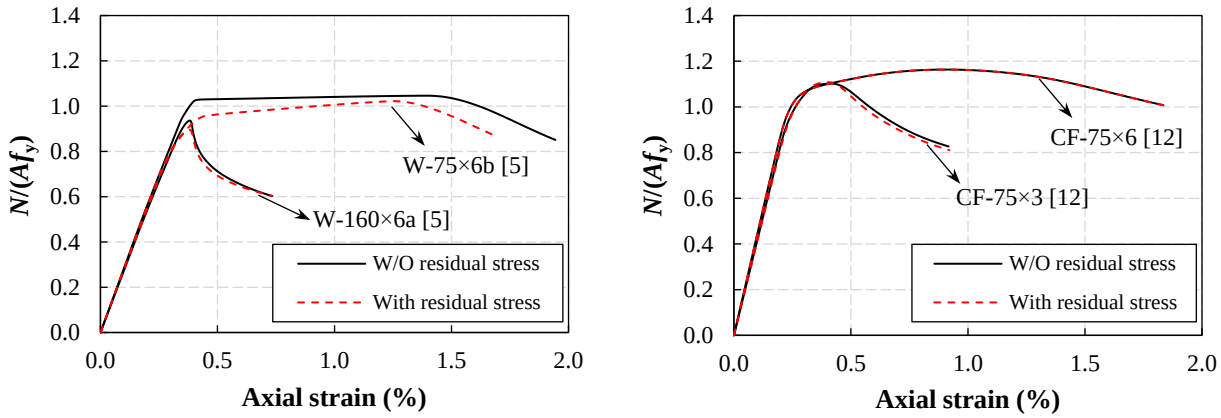

(a) Welded section (b) Cold-formed section

Fig. 7. Comparisons of FE results with and without residual stresses.

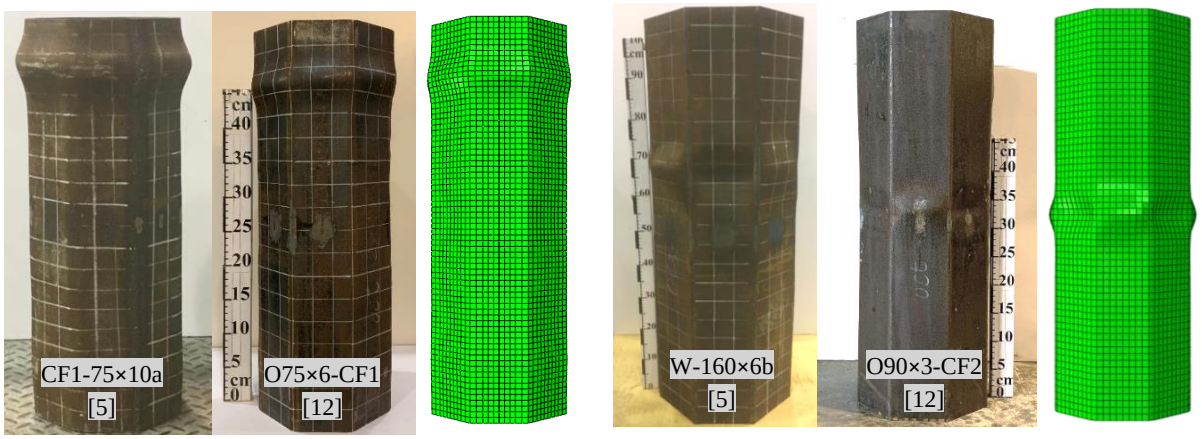

(a) Elephant foot buckling (b) Local buckling

Fig. 8. Typical failure modes from tests and corresponding FE models.

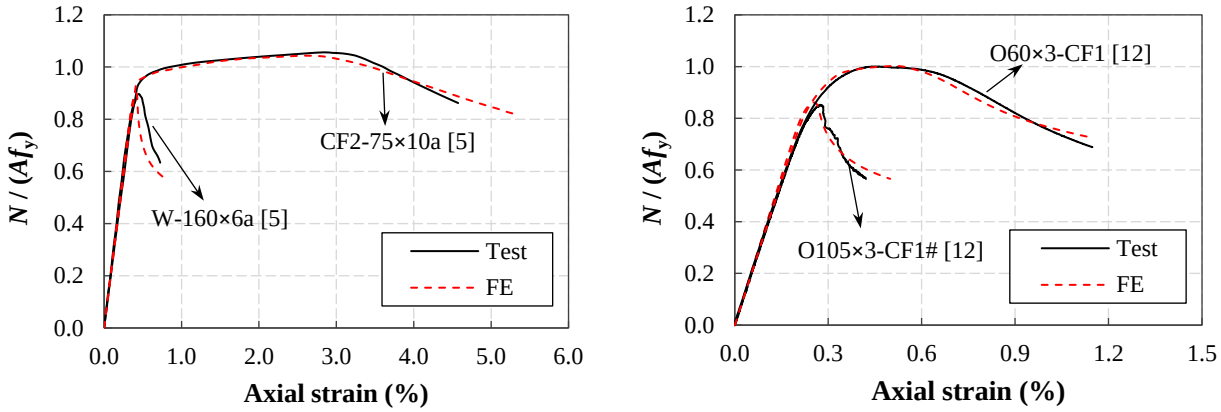

(a)Tests in [5] (b) Tests in [12]

Fig. 9. Comparisons of normalised axial load versus axial strain curves between tests and corresponding FE models.

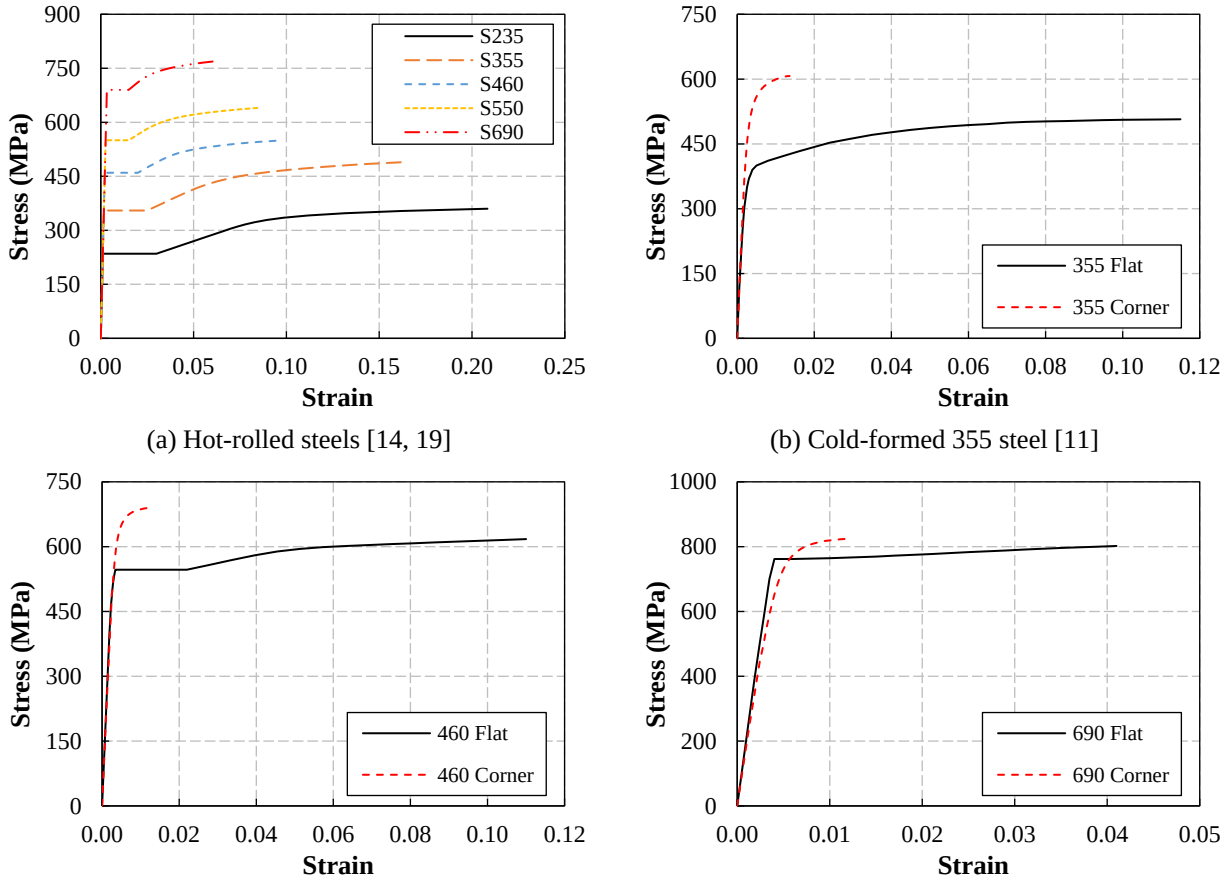

(a) Hot-rolled steels [14, 19]

(b) Cold-formed 355 steel [11]

(c) Cold-formed 460 steel [12]

(d) Cold-formed 690 steel [5]

Fig. 10. Material constitutive relationships used in the parametric study.

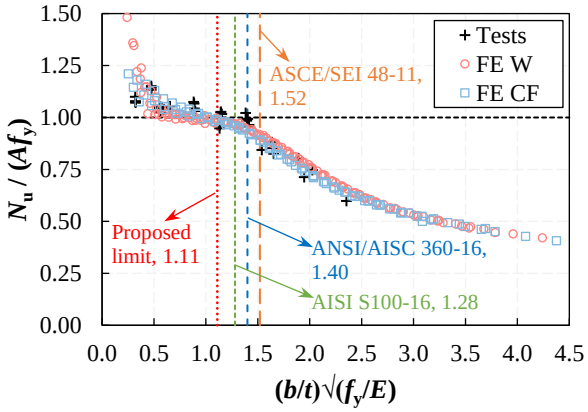

Fig. 11. Normalised ultimate load versus normalised slenderness parameter diagram.

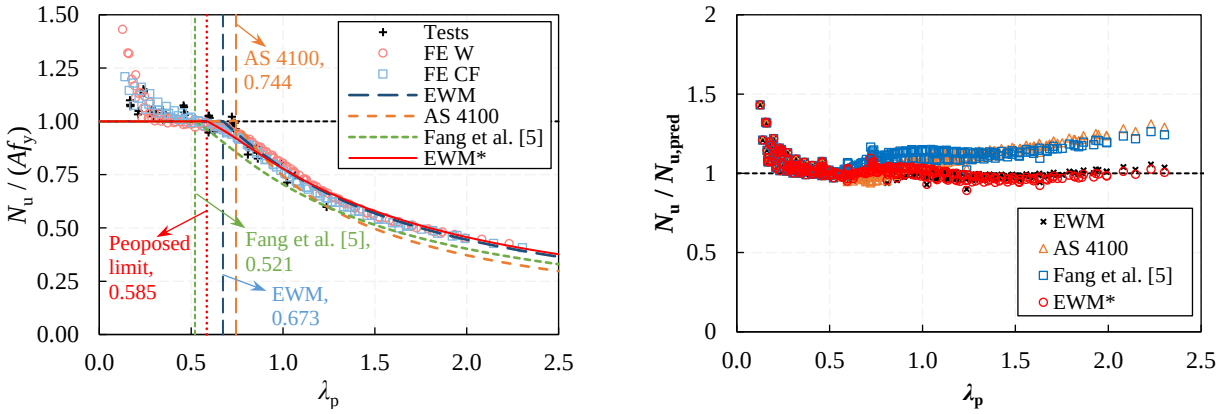

(a) (b)

Fig. 12. Comparison of test and FE results with EWM predictions.

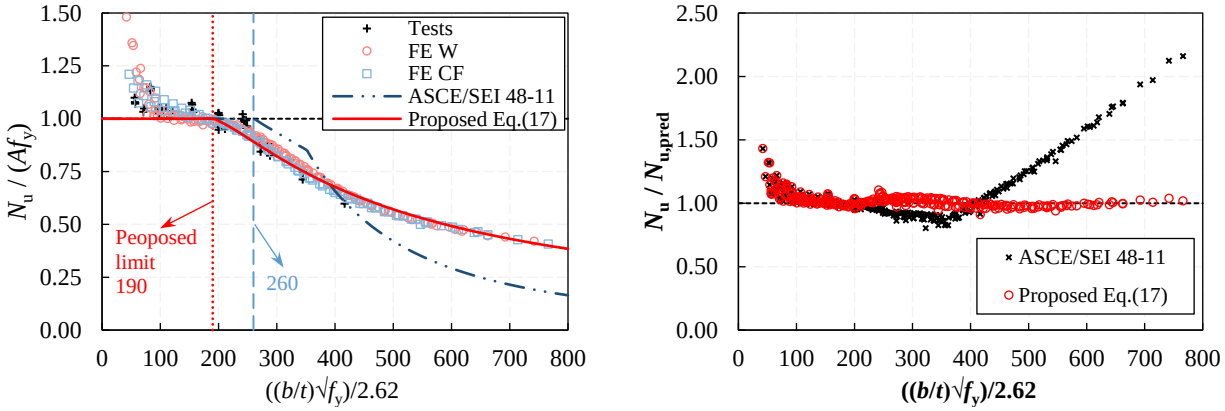

(a) (b)

Fig. 13. Comparison of test and FE results with ASCE/SEI 48-11 predictions.

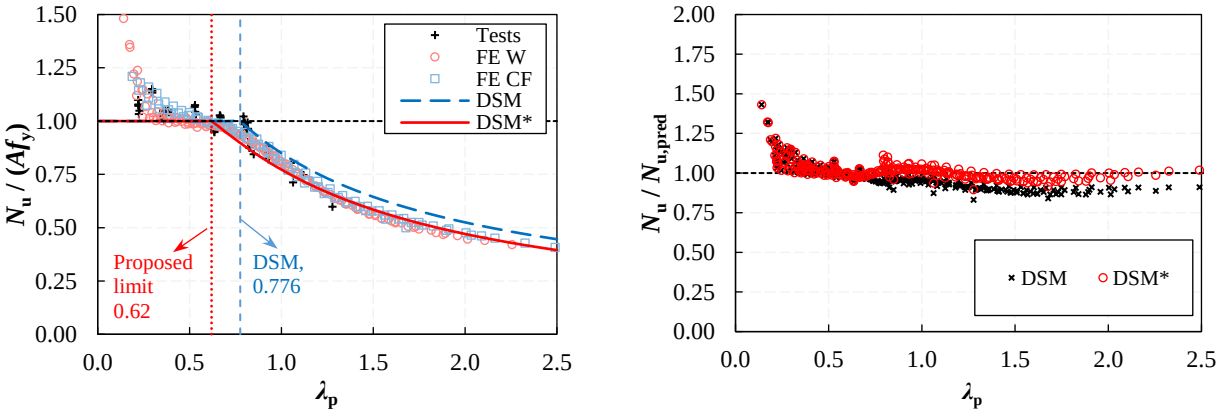

(a) (b)

Fig. 14. Comparison of test and FE results with DSM predictions.

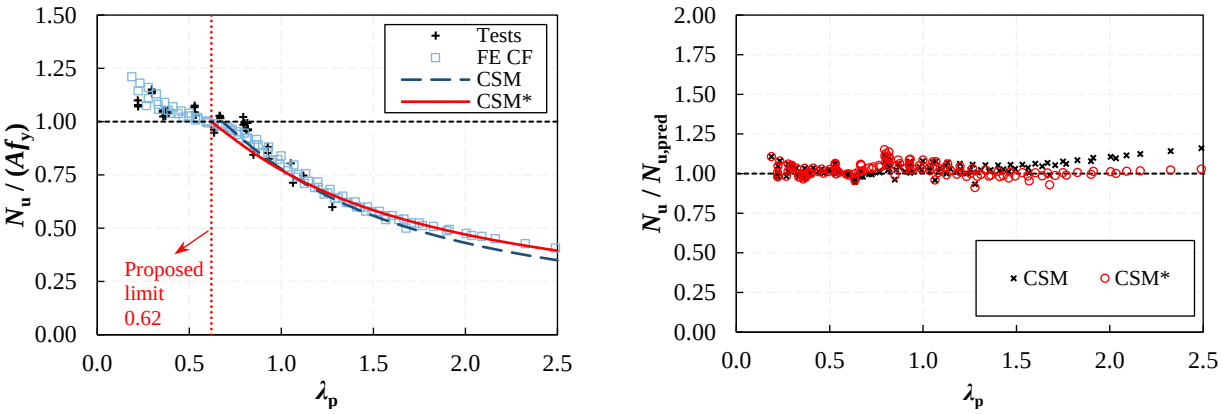

(a) (b)

Fig. 15. Comparison of test and FE results with CSM predictions.